Rotor Performance of an Isolated Full-Scale XV-15 Tiltrotor in Helicopter Mode

Mark D. Betzina
Aerospace Engineer, Army/NASA Rotorcraft Division
NASA Ames Research Center, Moffett Field, California
mbetzina@mail.arc.nasa.gov

Abstract

The performance of a full-scale XV-15 rotor operating in low-speed helicopter-mode flight on a rotor test apparatus was measured in the NASA Ames 80- by 120-Foot Wind Tunnel. The hub-tare-corrected results yield essentially isolated rotor performance minimally affected by the presence of the rotor test apparatus. These data comprise the most extensive data set published for a full-scale tiltrotor in low-speed helicopter-mode flight and can be used for validation of analytical techniques for the prediction of tiltrotor performance.

Notation

c_s	speed of sound, ft/sec
C_L	Rotor lift coefficient, $L / \rho(\Omega R)^2 \pi R^2$
C_Q	Rotor torque coefficient, $Q / \rho(\Omega R)^2 \pi R^3$
C_T	Rotor thrust coefficient, $T / \rho(\Omega R)^2 \pi R^2$
C_X	Rotor propulsive force coefficient, $-D / \rho(\Omega R)^2 \pi R^2$
D	Rotor drag, wind axis system, lb
F_M	Figure of merit, $(C_T^{3/2} / \sqrt{2}) / C_Q$
HF_{hub}	Rotor hub H-force tare, shaft axis system, lb
L	Rotor lift, wind axis system, lb
M_{tip}	Rotor tip Mach number, $\Omega R / c_s$
q	Dynamic pressure, $\rho V^2 / 2$, lb/ft^2
Q	Rotor torque, shaft axis system, ft-lb
Q_{hub}	Rotor hub torque tare, shaft axis system, ft-lb
R	Rotor radius, ft
T	Rotor thrust, lb
T_{hub}	Rotor hub thrust tare, shaft axis system, lb
V	Air velocity, ft/sec
V/ΩR	Advance ratio
α	Rotor shaft angle measured from vertical, positive aft, deg
ρ	Air density, slugs/ft^3
σ	Rotor thrust-weighted solidity
Ω	Rotor rotational speed, rad/sec
ΩR	Rotor tip speed, ft/sec

Presented at the American Helicopter Society Aerodynamics, Acoustics, and Test and Evaluation Technical Specialists Meeting, San Francisco, CA, January 23-25, 2002.

Introduction

The XV-15 tiltrotor research aircraft (Fig. 1) first flew in 1977, culminating a long period of tiltrotor technology development that began in the 1940's. Reference 1 provides a complete history of this aircraft that continues to be utilized for various tiltrotor research activities. Its 3-bladed, 25-ft diameter rotor provides a well-documented design suitable for evaluation of various analytical techniques applied to high-twist, high-solidity tiltrotors.

Fig. 1. XV-15 Tiltrotor Research Aircraft.

The highly twisted rotor blades used on tiltrotor aircraft provide good performance in airplane mode, when the rotor is operated as a propeller, but are not ideal for edgewise flight in helicopter mode. Therefore, tiltrotors have different characteristics in helicopter mode than typical helicopter rotors. Because of the high blade twist, the inboard portion of a tiltrotor generally produces more thrust compared to a helicopter rotor. In some descending flight conditions, the rotor tip may be negatively loaded, producing a pair of counter-rotating trailing vortices as

demonstrated by flow visualization of a small-scale V-22 rotor in Ref. 2. This situation provides a challenge for accurate performance prediction using existing analytical codes.

Wind tunnel testing is desired for accurate measurement of rotor performance because of the precise control over the operating conditions and the ability to directly measure the rotor forces and moments. However, very little wind tunnel data are available for full-scale tiltrotors in low-speed helicopter mode.

There have been several previous tests of full-scale XV-15 rotors. One was tested on a propeller test rig in the 40- by 80-Foot Wind Tunnel in 1970 (Ref. 3) for shaft angles from –15 to –90 deg and advance ratios above 0.18. The complete XV-15 aircraft was tested in the 40- by 80-Foot Wind Tunnel in 1978 (Ref. 4), but force and moment measurements included the contribution from the airframe. Hover performance of the XV-15 rotor is documented in Ref. 5. Reference 6 describes results from a single XV-15 rotor tested in the 80- by 120-Foot Wind Tunnel in hover and forward flight, but the forward flight data are limited to relatively few test conditions.

The data presented in the current paper comprise the most extensive data set published for a full-scale tiltrotor in low-speed helicopter-mode flight. These data can be used to validate and improve analytical codes, thereby advancing the state-of-the-art for tiltrotor performance prediction.

Experiment Description

Equipment

Rotor performance measurements were acquired in the NASA Ames 80- by 120-Foot Wind Tunnel on a full-scale XV-15 tiltrotor operating in helicopter mode. The right-hand XV-15 hub and rotor were installed on the NASA/Army Rotor Test Apparatus (RTA) as shown in Fig. 2. The RTA was supported by three struts as shown, placing the rotor hub approximately 31 ft (1.24 rotor diameters) above the floor. Shaft tilt was obtained by varying the height of the aft strut.

The RTA normally incorporates two 1500-horsepower electric motors, a right-angle speed-reducing transmission, and a 6-component rotor balance system. However, the RTA was modified to accommodate the higher rotational speed of the XV-15 rotor by removing the forward motor and installing an intermediate speed-increasing gearbox. A more detailed description of the RTA and its rotor balance system is available in Ref. 7. The primary dimensions of the RTA are shown in Fig. 3.

The swashplate, pitch links, and pitch arms were slightly different from the aircraft hardware. In particular, the trailing pitch-arm/pitch-link arrangement had a pitch-up/flap-up coupling of 36 deg (δ_3 = -36 deg), whereas δ_3 is -15 deg on the aircraft. Also, the test configuration included an instrumentation hat above the hub and did not include a hub spinner. General properties of the XV-15 rotor are shown in Table 1. More detailed rotor geometry can be found in Ref. 5.

Fig. 2. XV-15 rotor on the Rotor Test Apparatus in the NASA Ames 80- by 120-Foot Wind Tunnel.

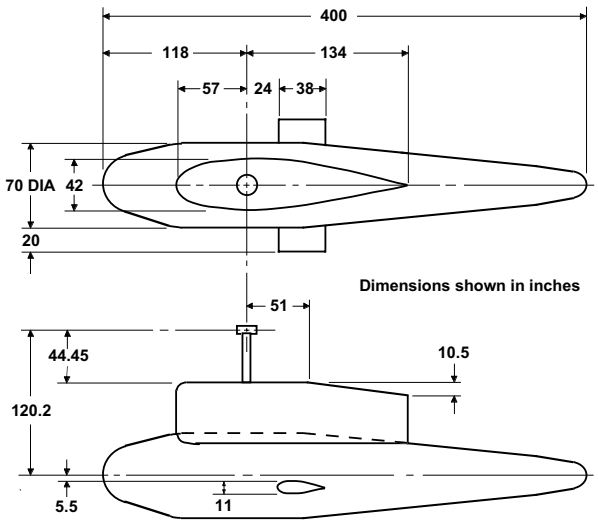

Fig. 3. Dimensions of Rotor Test Apparatus.

Table 1. Rotor Properties

Parameter	Value
Number of blades	3
Rotor radius, R, ft	12.5
Blade chord (constant), ft	1.167
Rotor solidity (thrust weighted), σ	0.089
Blade twist (non-linear), deg	-40.9
Hub precone, deg	1.5

Test Conditions

The test conditions are shown in Table 2. The typical test procedure varied shaft angle while maintaining constant advance ratio ($V/\Omega R$), constant thrust coefficient (C_T), and constant tip Mach number (M_{tip}). The shaft angle was varied from –15 to 15 deg, simulating a wide range of both propulsive and descending helicopter-mode flight conditions. All data presented in this paper were acquired with the first harmonic flapping trimmed to zero (± 0.1 deg) by adjusting cyclic pitch. Therefore, the rotor tip-path-plane angle-of-attack and the rotor shaft angle (α) were essentially equal.

Table 2. Test Conditions

Parameter	Value
Tip Mach number, M_{tip}	0.691
Advance ratio, $V/\Omega R$	0, 0.125, 0.15, 0.17, 0.20
Shaft angle, α, deg	-15 to 15
Thrust coefficient to solidity ratio, C_T/σ	0.06 to 0.12

Data Acquisition and Reduction

Rotor balance signals were low-pass filtered at 100 Hz and sampled synchronously with the rotor speed at 64 samples per revolution (approximately 630 Hz) per channel. Each data point consisted of 4096 samples (64 revolutions) for each rotor-balance component which were averaged to yield mean forces and moments in the balance axis system. These forces and moments were corrected for weight tares and then transferred to both shaft-axis and wind-axis reference systems, using the hub centerline as the moment center.

Rotor Balance Accuracy

Based on an extensive calibration, standard deviations of the measured load from the applied load were previously determined to be 25 lb for thrust, 7 lbs for H-force, and 10 ft-lb for torque. Thrust, H-force, and torque checkloads performed during the current test verified accuracy within the stated standard deviations and confirmed the calibration slopes within 0.08% for thrust, 0.72% for H-force, and 0.22% for torque.

Wall Effects

Using the method described in Ref. 8, downwash corrections to the shaft angle were estimated to be less than 0.5 deg for the test conditions presented in this paper. Therefore, wall corrections were not applied to the data.

Hub Tares

The rotor-balance measurements included contributions from the hub hardware. To obtain isolated-rotor data, hub tares that included the aerodynamic forces and moments generated by the rotating hub, pitch links, scissors, swashplate, and shaft were subtracted from the measured rotor performance data. The hub tares do not include the mutual interference effects between the hub and rotor. However, because the hub tares are quite small, this error is considered negligible.

The hub tares were determined from both measured data with the rotor blades removed and estimates of the contributions from the blade spindles and pitch links. Estimates for the blade spindles, which contributed to the measured blades-off data, were required because they were not exposed during blades-on operation. Figure 4 shows a close-up view of the hub configuration with the blades installed. Figure 5 shows the exposed blade spindles with the blades removed. Estimates for the pitch links were required because they had to be removed during blades-off operation.

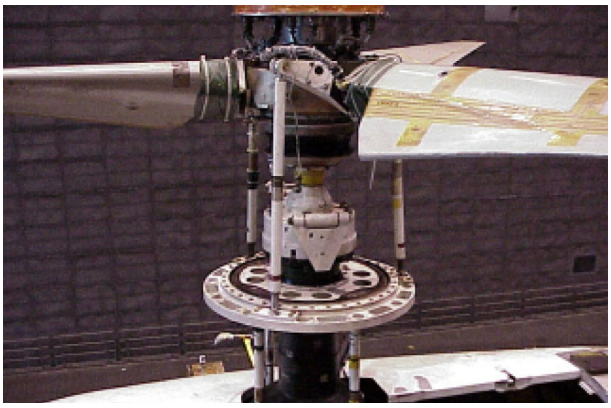

Fig. 4. Rotor hub with blades installed.

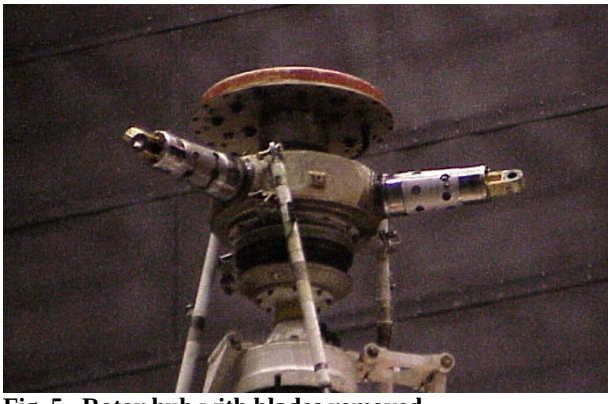

Fig. 5. Rotor hub with blades removed.

Drag coefficients as a function of radius were estimated for the spindles and pitch links using Ref. 9. CAMRAD II (Ref. 10) was then used to determine the contributions of the spindles and pitch links to the thrust, H-force, and torque of the rotating hub in forward flight. Corrected hub tares were obtained by subtracting the contribution of the spindles and adding the contribution of the pitch links to the measured blades-off data. Blades-off data were obtained for all combinations of dynamic pressure and shaft angle used during the test.

The following equations were used to curve-fit the corrected hub tares:

$$T_{hub} = 2.77 + 0.5193q + 0.4565\alpha + 0.09340q\alpha - 0.00755\alpha^2$$

$$HF_{hub} = 2.46 + 4.0702q - 0.4193\alpha - 0.01392q\alpha - 0.02175\alpha^2 - 0.000630q\alpha^2$$

$$Q_{hub} = 70.04 + 0.2001q + 0.001923q^2 - 0.2869\alpha + 0.00432q\alpha$$

where T_{hub}, HF_{hub}, and Q_{hub} are the hub tares for thrust, H-force, and torque, respectively. These equations are valid only for dynamic pressures between 10 and 32 lb/ft^2 and shaft angles from –15 and 15 deg.

Figures 6-11 show the corrected hub tares and the blades-off data. Figure 6 presents the hub thrust tare versus dynamic pressure for zero shaft angle. Figure 7 presents the thrust tare versus shaft angle for an intermediate dynamic pressure of 21.2 lb/ft^2. Similarly, Figs. 8-11 present the H-force and torque tares. As shown, the correction for the spindles and pitch links is relatively small compared with the measured blades-off data.

In hover, the blades-off data indicated negligible values of thrust and H-force, but a torque of approximately 80 ft-lb. Therefore, only a torque tare was applied to the hover data. The CAMRAD II estimates of spindle torque and pitch link torque were approximately 14 ft-lb and 4 ft-lb, respectively, yielding a corrected hover torque tare of 70 ft-lb. The larger-than-expected blades-off torque indicated that it included both aerodynamic torque and an apparent rotational effect on the torque measurement.

Influence of the Rotor Test Apparatus on Rotor Performance

The data were not corrected for interference effects caused by the presence of the RTA body. Analytical estimates of the body's influence on rotor performance were shown to be very small for representative helicopter rotors in Ref. 11. However, because the XV-15 rotor had a smaller diameter and higher disk loading than the helicopter rotors typically tested on the RTA, computations were performed to quantify the influence of the RTA body using CAMRAD II.

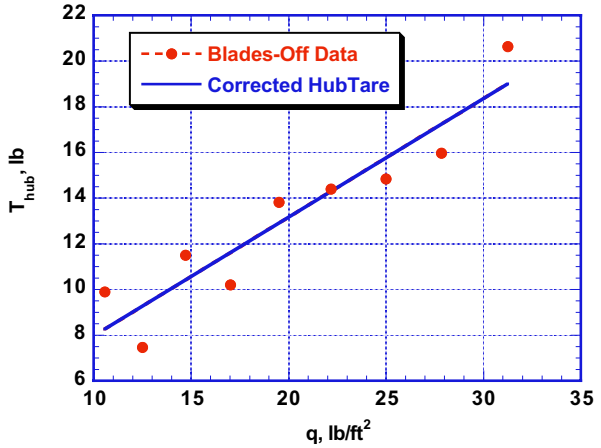

Fig. 6. Effect of dynamic pressure on hub thrust tare, α = 0 deg.

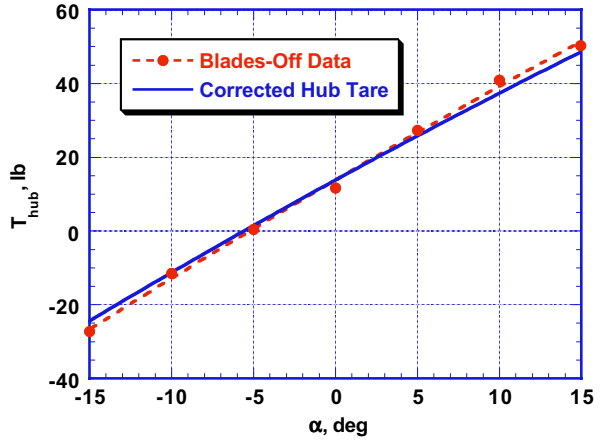

Fig. 7. Effect of shaft angle on hub thrust tare, q = 21.2 lb/ft^2.

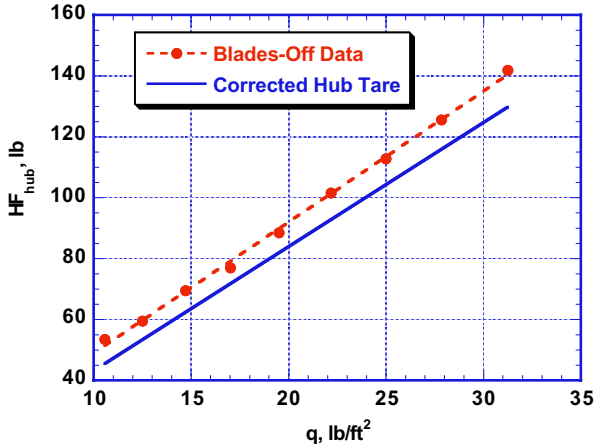

Fig. 8. Effect of dynamic pressure on hub H-force tare, α = 0 deg.

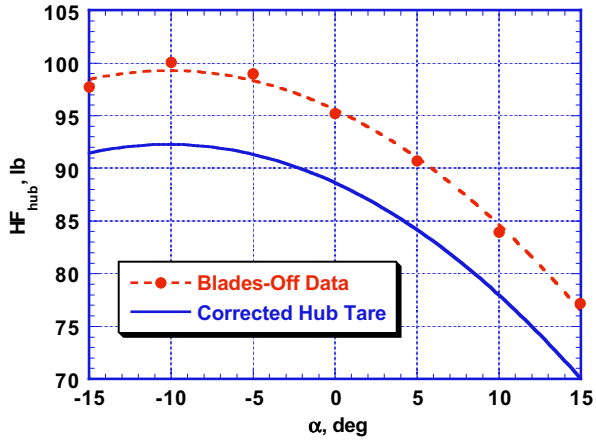

Fig. 9. Effect of shaft angle on hub H-force tare, q = 21.2 lb/ft^2.

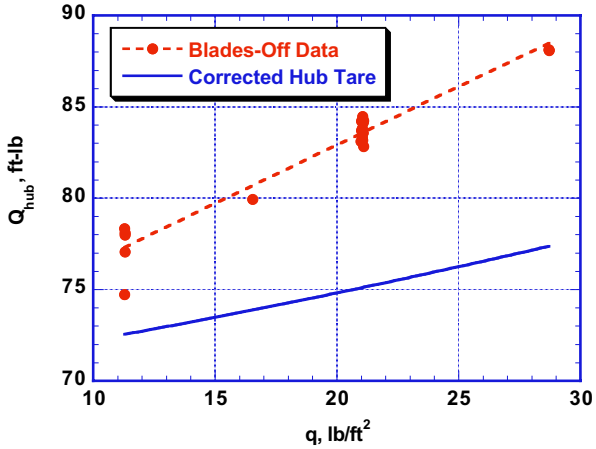

Fig. 10. Effect of dynamic pressure on hub torque tare, α = 0 deg.

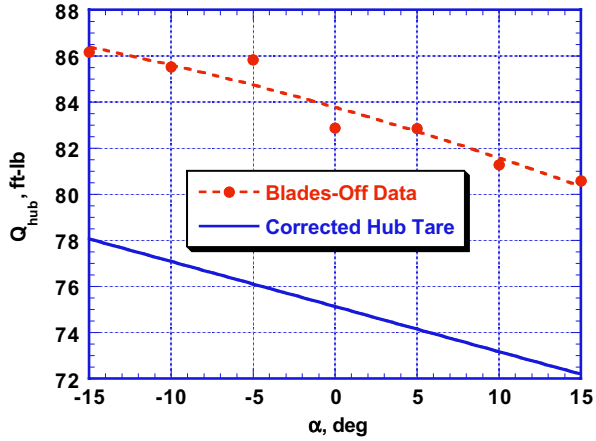

Fig. 11. Effect of shaft angle on hub torque tare, q = 21.1 lb/ft^2.

Computations performed with and without the presence of the RTA at the same thrust coefficient revealed that the effect on the rotor's propulsive force was negligible, but that rotor torque was slightly affected. The effect on torque coefficient is shown in Figs. 12 and 13, where the computed difference in torque coefficient was subtracted from the tare-corrected data to show an estimate of the rotor torque coefficient without the RTA influence (dashed lines). Figure 12 shows torque coefficient as a function of thrust coefficient at constant advance ratio. Figure 13 shows torque coefficient as a function of advance ratio at constant thrust coefficient. The largest differences occurred at a shaft angle of –15 deg, where the presence of the RTA caused a slight reduction in measured torque for the same thrust coefficient and advance ratio.

For the most accurate correlation of analytical codes with the data presented in this paper, it is recommended that the presence of the RTA be included in the analysis. However, Figs. 12 and 13 indicate that ignoring the presence of the RTA will yield only minor errors.

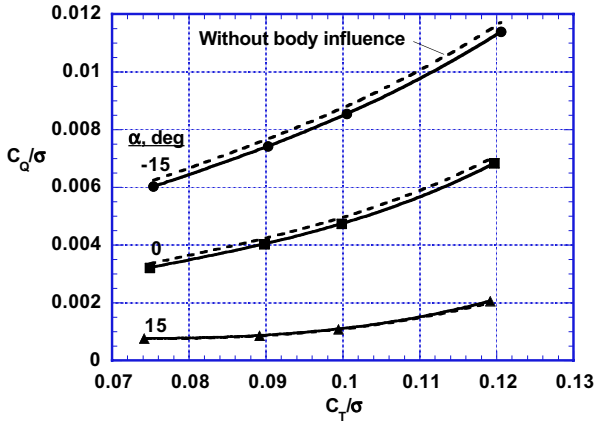

Fig. 12. Effect of RTA body on rotor torque coefficient, V/ΩR = 0.15.

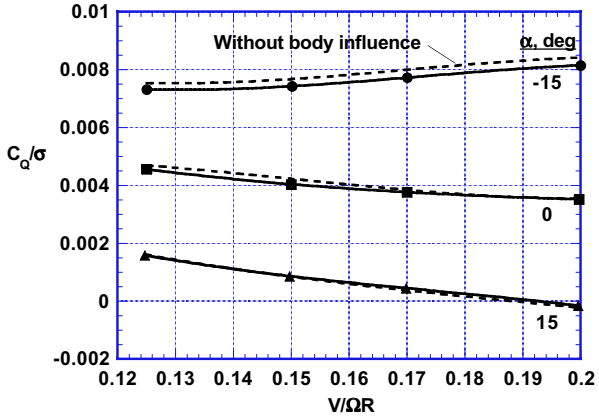

Fig. 13. Effect of RTA body on rotor torque coefficient, C_T/σ = 0.09.

Results

Hover Performance

The hover figure of merit is compared with previous test results (Refs. 5 and 6) in Fig. 14. As described above, the hover data have been corrected for the hub torque tare. The current test results compare very well with the 80- by 120-Foot Wind Tunnel data from Ref. 6, but show a slight reduction (about 3.5%) in maximum figure of merit relative to the data obtained at the Outdoor Aerodynamic Research Facility (OARF) reported in Ref. 5. This is consistent with expected facility effects on hover performance measurements (Ref. 12). Figure 15 shows hover torque coefficient versus thrust coefficient, with both coefficients normalized by the rotor solidity (σ). The data points shown in Figs. 14 and 15 are from two different runs, indicating good repeatability.

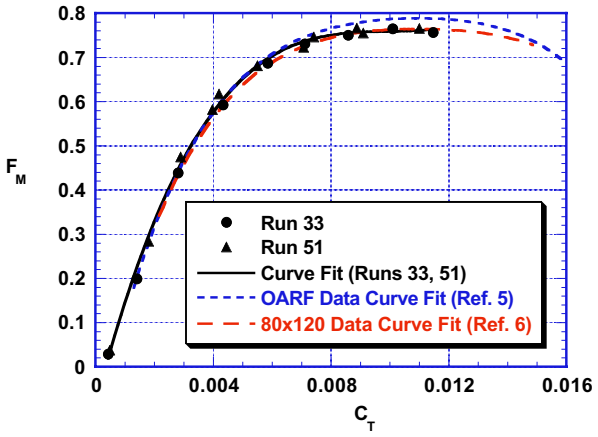

Fig. 14. Hover performance comparison with previous data.

Forward Flight Performance

All coefficients have been normalized by the rotor solidity (σ) in the following figures. Figure 16 shows torque coefficient as a function of advance ratio for a constant C_T/σ of 0.075 and compares the current test results (open symbols) with previous XV-15 rotor performance data (Refs. 3 and 6). There is only one point from the 1970 data of Ref. 3 that is near the test conditions of the current test. This point was obtained by interpolating the data from a thrust sweep at a shaft angle of –14.5 deg. and an advance ratio of 0.182. The current test indicates higher torque than reported in Ref. 3, but consistently lower torque than reported in Ref. 6. As discussed in Ref. 6, the large discrepancy between Refs. 3 and 6 may have been partly due to the proximity of the wind-tunnel ceiling to the rotor at a shaft angle of –15 deg in the 40- by 80- Foot Wind Tunnel used in Ref. 3. The current test results reduce this discrepancy to about half as much, which is more consistent with the expected wall-effect discussed in Ref. 6. However, because Ref. 6 used the same test hardware in the same facility as the current test, the source of the discrepancy with Ref. 6 was investigated further.

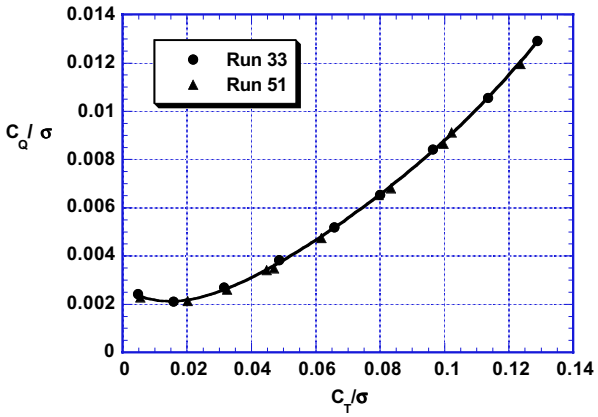

Fig. 15. Hover torque coefficient versus thrust coefficient.

The difference shown in Fig. 16 between the current results and Ref. 6 represents a torque of 175-485 ft-lb. Hub tares were not applied to the data in Ref 6, but this accounts for only about 75 ft-lb of the total difference. Primary and back-up torque gages were recorded for both tests. The primary torque measurement was found to be unreliable during the current test, showing inaccurate results with the checkloads and significant zero shifts throughout the test. As a result, the current test relied exclusively on the back-up torque measurement. However, the data in Ref. 6 is based on the primary torque measurement. Further investigation of the prior test data (Ref.6) revealed that a similar behavior of zero shifts on the primary torque measurement occurred during that test. Therefore, the Ref. 6 data in Fig. 16 was re-computed using the back-up torque measurement corrected for the hub torque tare. The result is compared with the current data in Fig. 17. The discrepancy between the two tests is

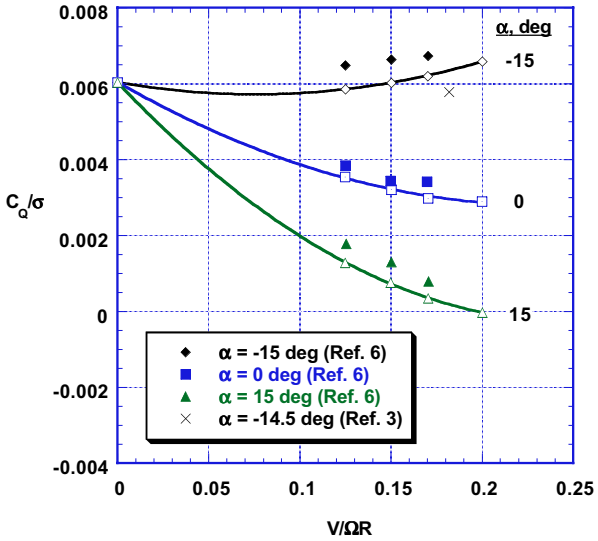

Fig. 16. Comparison with previous data, torque coefficient versus advance ratio, nominal $C_T/\sigma = 0.075$.

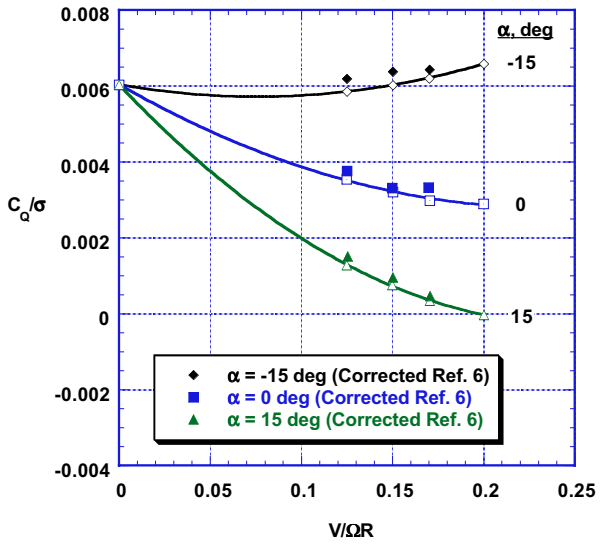

Fig. 17. Comparison with corrected Ref. 6 data, torque coefficient versus advance ratio, nominal $C_T/\sigma = 0.075$.

reduced considerably, but the torque shown for the current test remains consistently lower than Ref. 6.

As a result of these findings, the hover data from Ref. 6 shown in Fig. 14 was also recomputed using the back-up torque measurement. However, during the hover runs of that test, the difference between the primary and back-up torque measurements was negligible. Therefore, it appears that the hover data presented in Ref. 6 are accurate. Although the hover data from the current test compare well with Ref. 6, there is an unexplained torque discrepancy in forward flight of 70-270 ft-lb. An attempt to determine the source of this remaining discrepancy was unsuccessful.

Torque coefficients versus both thrust coefficient and lift coefficient are shown in Figs. 18 and 19, respectively, for various shaft angles at each of the advance ratios tested. The dashed lines are curve fits of the data without hub tare subtraction, indicating that the hub tare correction is very small.

Figure 20 presents lift coefficient versus propulsive force coefficient. Again, the dashed lines are curve-fits of the data without hub tare subtraction, indicating that the hub tare correction for propulsive force is more significant, especially at the higher advance ratios.

The forward-flight data presented in this paper were acquired during six different wind-tunnel runs over a 2-month period. To verify satisfactory data repeatability, a data point was acquired at similar test conditions at the beginning and end of each run. The test condition used for this check was 0.125 advance ratio, α = 0 deg, at a nominal C_T/σ of 0.075. All of these points are shown in Figs. 18a, 19a, and 20a. To better quantify the deviations between these points, the regions of Figs. 18a and 20a showing these points are expanded in Fig. 21. The maximum deviations of C_Q/σ and C_X/σ from the curve-fits are 0.00006 and 0.0009, respectively.

Using the curve-fits shown in Figs. 19 and 20 to interpolate the tare-corrected data, plots of torque coefficient versus propulsive force coefficient are presented in Fig. 22 for various shaft angles and lift coefficients.

Conclusions

The performance of a full-scale XV-15 tiltrotor in helicopter mode was measured in the NASA Ames 80- by 120-Foot Wind Tunnel. The data comprise the most extensive data set published for a full-scale tiltrotor in low-speed helicopter-mode flight and can be used to validate analytical codes. Specific findings include the following:

1. Analytical estimates of the effect of the Rotor Test Apparatus (RTA) body on measured rotor performance revealed relatively minor effects on rotor torque, the largest of which occurred at a shaft angle of –15 deg. It is recommended that the RTA be included in the analysis for the most accurate correlation with these data.

2. The hover data compare well with previous test results in the same facility (Ref. 6). The forward-flight data show slightly lower torque than the earlier test in the same facility (Ref. 6) but slightly higher torque than a 1970 test in the 40- by 80-Foot Wind Tunnel (Ref 3).

3. As expected, the hub tares were shown to be relatively small except for the propulsive force correction, which increased as the advance ratio increased.

4. Data repeatability at the same thrust coefficient was shown to be within 0.00006 for C_Q/σ and within 0.0009 for C_X/σ.

Acknowledgement

The author expresses sincere gratitude to Dr. Wayne Johnson for providing CAMRAD II computations of the RTA influence on rotor performance as well as computations to support hub tare development.

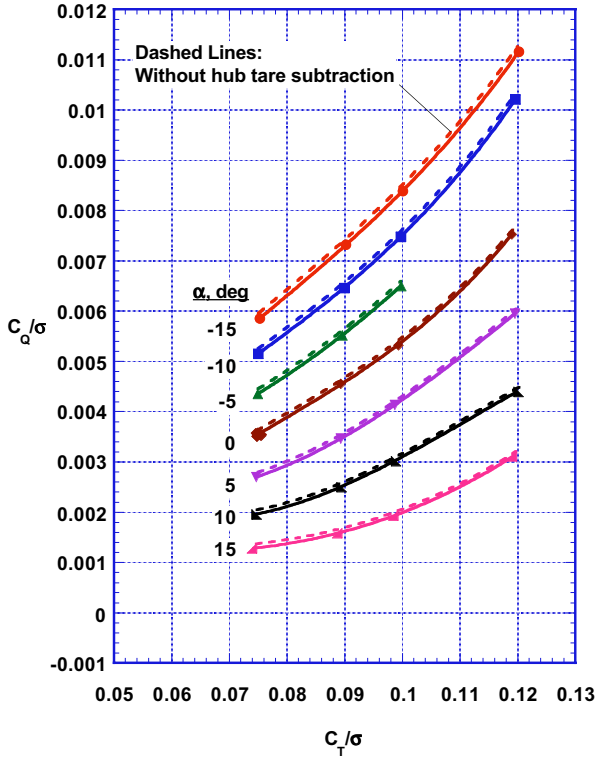

a) V/ΩR = 0.125

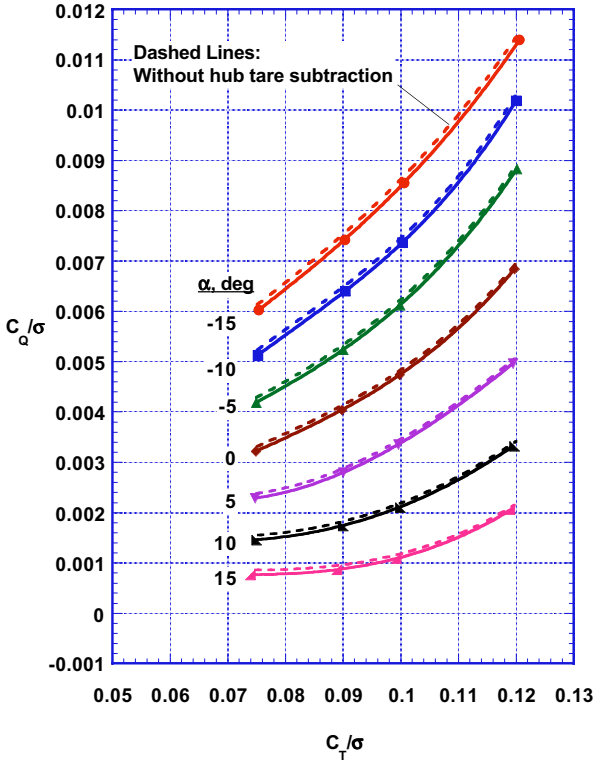

b) V/ΩR = 0.15

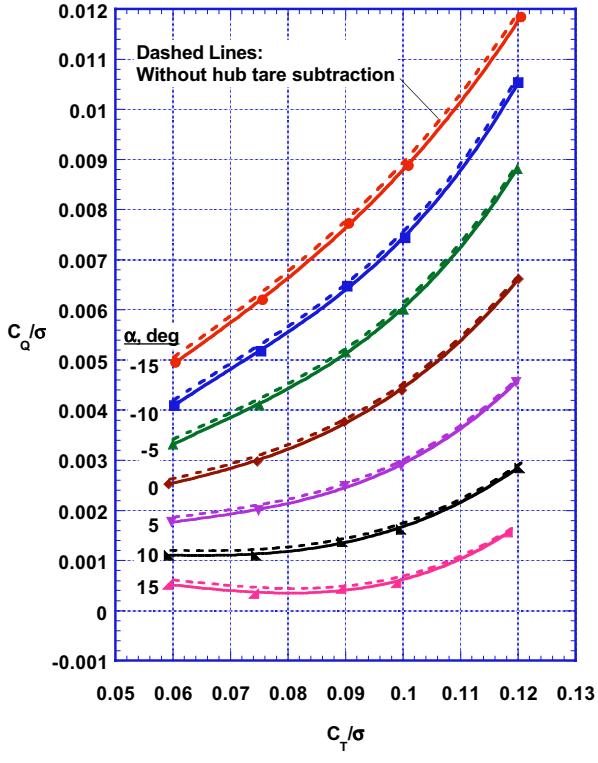

c) V/ΩR = 0.17

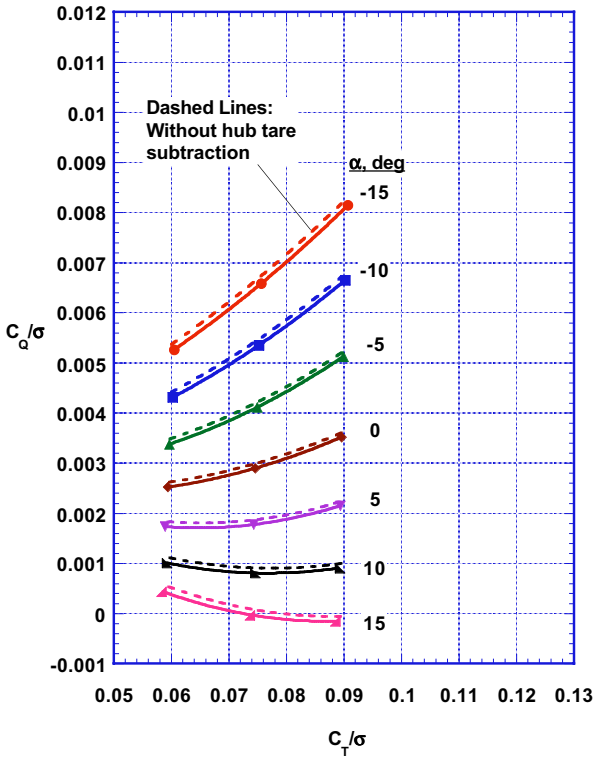

d) V/ΩR = 0.20

Fig. 18. Torque coefficient versus thrust coefficient.

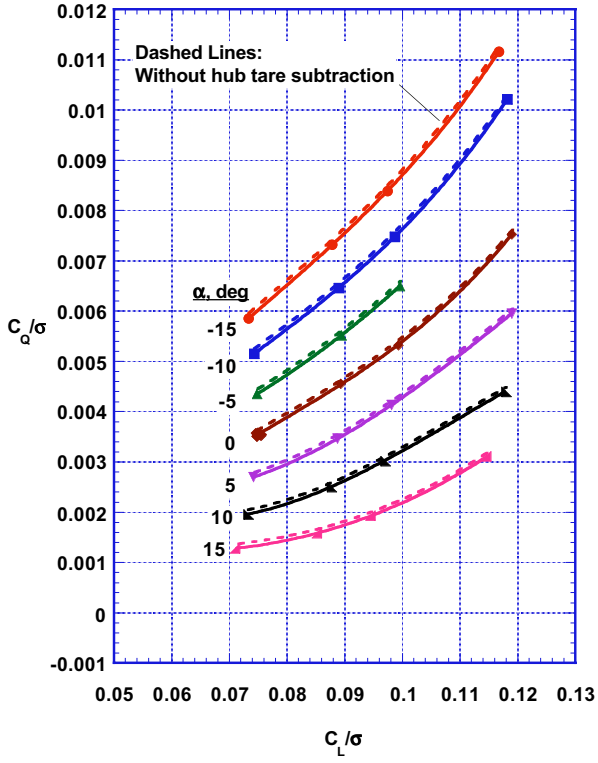

a) V/ΩR = 0.125

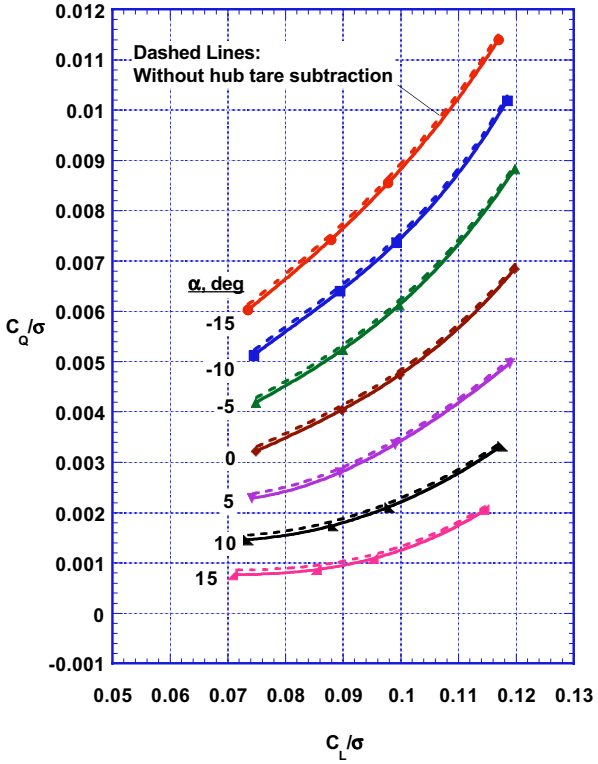

b) V/ΩR = 0.15

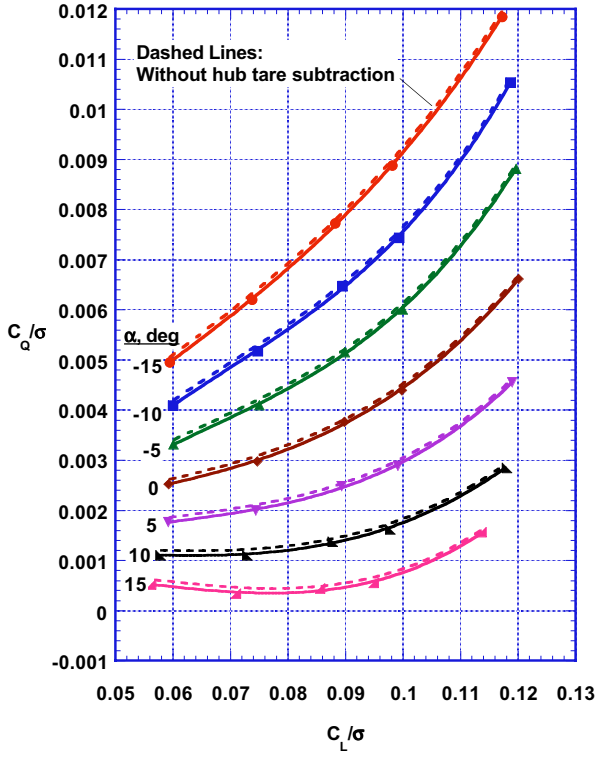

c) V/ΩR = 0.17

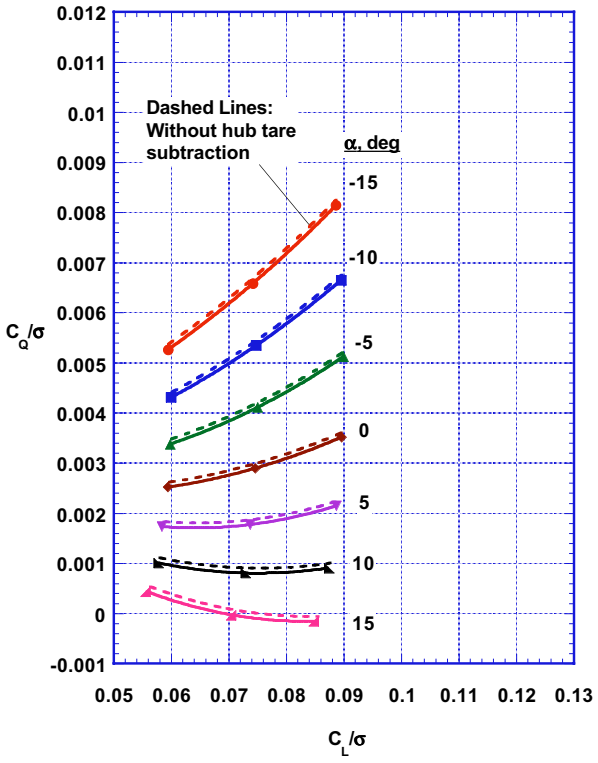

d) V/ΩR = 0.20

Fig. 19. Torque coefficient versus lift coefficient.

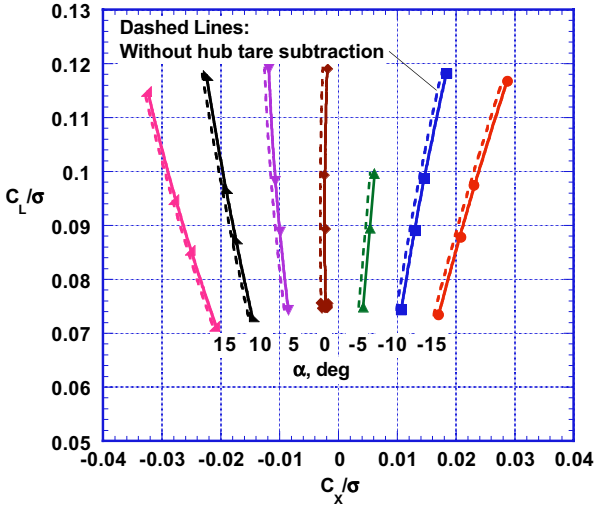

a) V/ΩR = 0.125

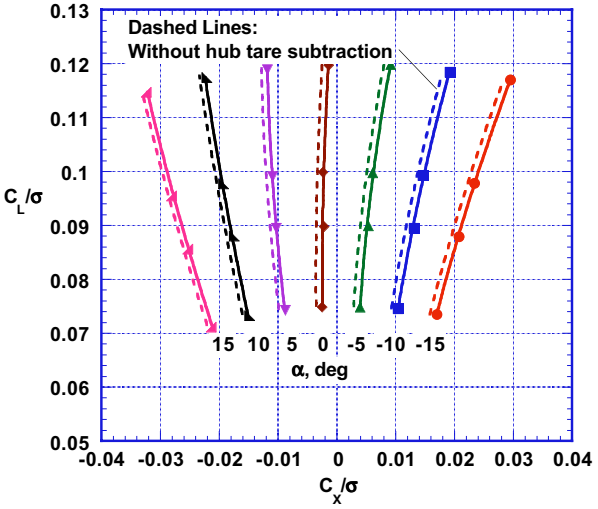

b) V/ΩR = 0.15

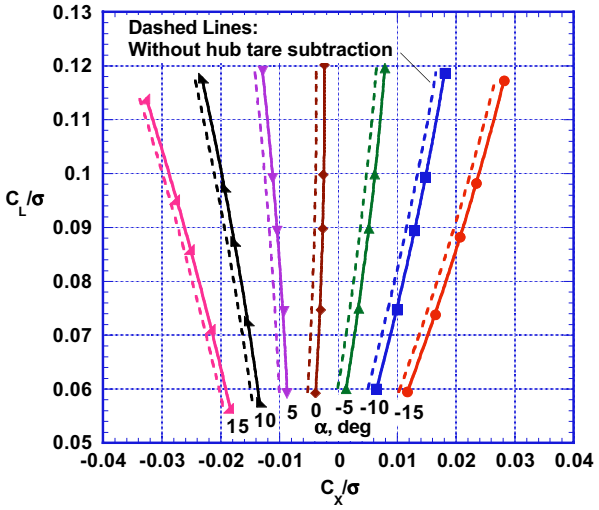

c) V/ΩR = 0.17

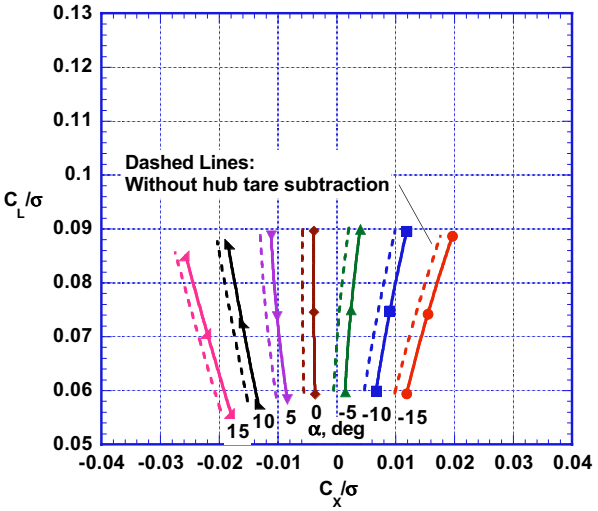

d) V/ΩR = 0.20

Fig. 20. Lift coefficient versus propulsive force coefficient.

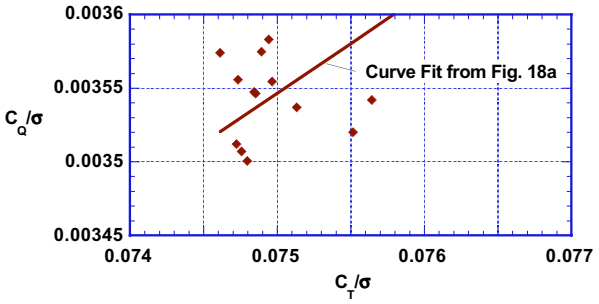

a) Torque coefficient versus thrust coefficient.

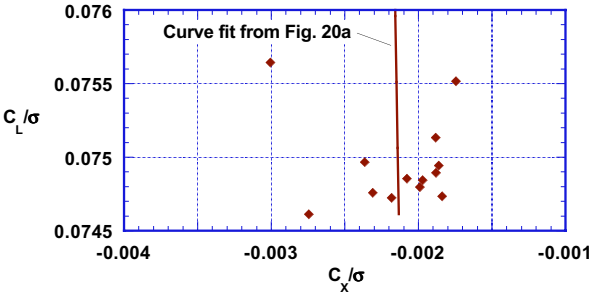

b) Lift coefficient versus propulsive force coefficient.

Fig. 21. Data Repeatability, V/ΩR = 0.125, α = 0 deg.

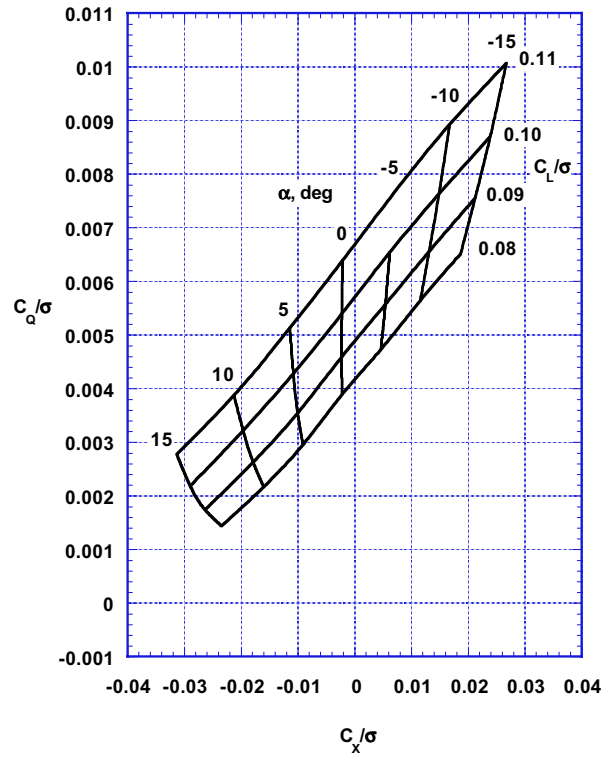

a) V/ΩR = 0.125

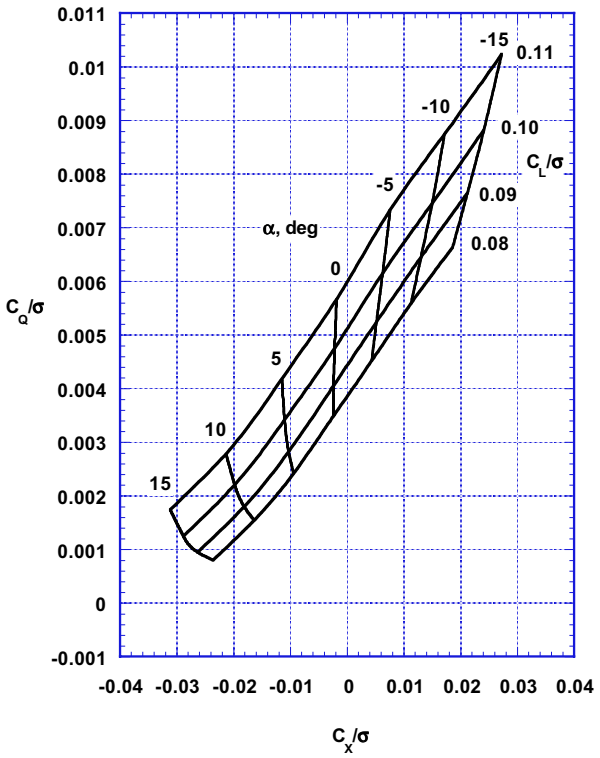

b) V/ΩR = 0.15

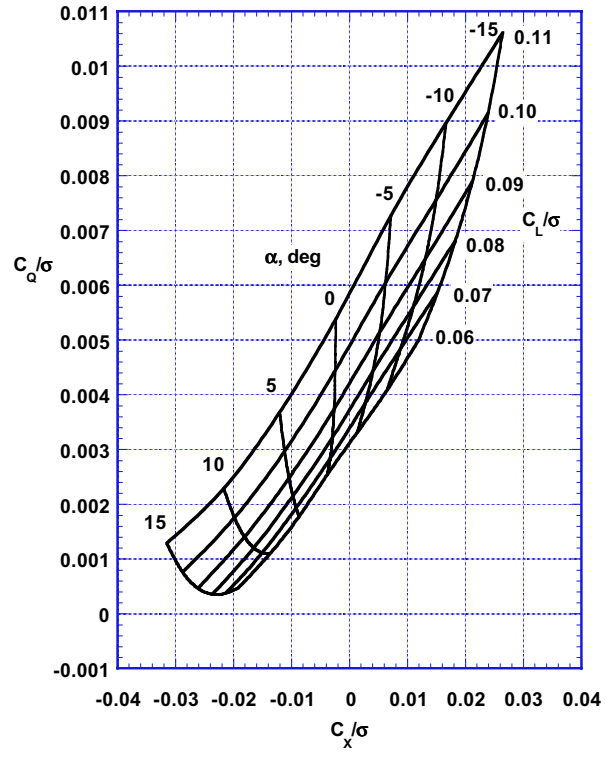

c) V/ΩR = 0.17

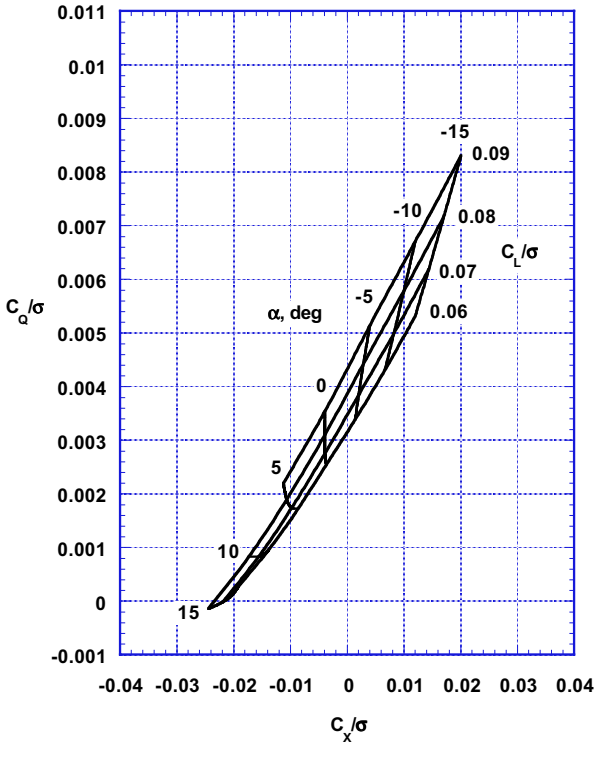

d) V/ΩR = 0.20

Fig. 22. Torque coefficient versus propulsive force coefficient.

References

1. Maisel, M. D., Giulianetti, D. J., Dugan, D. C., "The History of the XV-15 Tilt Rotor Research Aircraft: From Concept to Flight," NASA SP-2000-4517, 2000.

2. Yamauchi, G., Burley, C., Mercker, E., Pengel, K., and JanakiRam, R., "Flow Measurements of an Isolated Model Tilt Rotor," American Helicopter Society 55th Annual Forum, Montreal, Canada, May 1999.

3. "Advancement of Proprotor Technology, Task II – Wind-Tunnel Test Results," NASA CR 114363, September 1971.

4. Weiberg, J. A., Maisel, M. D., "Wind-Tunnel Tests of the XV-15 Tilt Rotor Aircraft," NASA TM 81177, April 1980.

5. Felker, F. F., Betzina, M. D., Signor, D. B., "Performance and Loads Data from a Hover Test of a Full-Scale XV-15 Rotor," NASA TM 86833, November 1985.

6. Light, J. S., "Results from an XV-15 Rotor Test in the National Full-Scale Aerodynamics Complex," American Helicopter society 53rd Annual Forum, Virginia Beach, Virginia, April 1997.

7. Norman, T. R., Cooper, C. R., Fredrickson, C. A., Herter, J. R., "Full-Scale Wind Tunnel Evaluation of the Sikorsky Five-Bladed Bearingless Main Rotor," American Helicopter Society 49th Annual Forum, St. Louis, Missouri, May 1993.

8. Rae, W. H., Pope, A., Low-Speed Wind Tunnel Testing, Second Edition, John Wiley & Sons, Inc., New York, 1984, pp. 376-385.

9. Hoerner, S. F., Fluid-Dynamic Drag, Published by the Author, New Jersey, 1965, pp. 3-9, 3-17.

10. Johnson, W. "CAMRAD II, Comprehensive Analytical Model of Rotorcraft Aerodynamics and Dynamics," Johnson Aeronautics, Palo Alto, CA, 1992-1997.

11. Yamauchi, G., Johnson, W., "Development and Application of an Analysis of Axisymmetric Body Effects on Helicopter Rotor Aerodynamics Using Modified Slender Body Theory," NASA TM 85934, July 1984.

12. Shinoda, P., Johnson, W., "Performance Results from a Test of an S-76 Rotor in the NASA Ames 80- by 120-Foot Wind Tunnel," AIAA-93-3414, AIAA Applied Aerodynamics Conference, Monterey, CA, August 1993.